Regular Article

PHYSICAL CHEMISTRY RESEARCH
Published by the
Iranian Chemical Society
www.physchemres.org
info@physchemres.org

Phys. Chem. Res., Vol. 11, No. 3, 501-510, September 2023
DOI: 10.22036/pcr.2022.343436.2110

Structural, Optical, and Luminescence Studies of Sm_2O_3-Doped $Cd_2Sr(PO_4)_2$ Nanopowder

K. Srinivasa Rao[a,b], K. Venkatarao[a,c], Y. Nirmal Rajeev[a,d] and S. Cole[a,*]
[a]*Department of Physics, Acharya Nagarjuna University, Guntur-522510, India*
[b]*Department of Physics, Government Degree College, Palakonda-532440, India*
[c]*Department of Physics, Government Institute of Textile Technology, Guntur-522005, India*
[d]*Department of Physics, V. R. Siddhartha Engineering College (A), Kanuru, Vijayawada-520007, A.P. India*
(Received 21 May 2022, Accepted 29 July 2022)

The present work aimed to study the structural and optical properties of cadmium strontium phosphate nanopowder (CSP) prepared by the solid state reaction (SSR) method, which is a well-known commercial and conventional synthesis technology to synthesize nanopowders. To study the nature of the prepared samples, various characterization techniques, including powder X-ray diffraction studies (P-XRD), scanning electron microscopy (SEM) with energy-dispersive X-ray spectroscopy, diffuse reflectance spectroscopy (DRS), Fourier transform infrared spectroscopy (FT-IR), and photoluminescence studies were utilized. The P-XRD revealed an average crystallite size of 15 nm. SEM micrographs revealed non-uniform biscuit-shaped flakes for the prepared sample. The band gap value of the prepared nanopowder estimated by the DRS study was 5.3 eV. FT-IR confirmed the presence of ions related to the phosphate group in the prepared nanopowder. Based on the PL spectrum, the prepared sample exhibited an intense emission at 596 nm upon excitation at 401 nm. Color purity, color rendering index, and color-correlated temperature were also calculated and are reported in the article.

Keywords: Nanopowder, Solid state reaction, Cadmium, Strontium, Diffuse reflectance spectroscopy, Color purity

INTRODUCTION

Recently, light-emitting diodes (LEDs) have received more attention from researchers due to their vast range of applications, multiple benefits, and extensive use in quickly advancing technology [1]. LEDs' low power consumption, sturdy construction, compact size, and quick response have made them particularly attractive to both researchers and consumers [2-3]. Nanopowder is currently undergoing extensive processing. For decades, aluminates, silicates, and nitrides based nanopowders have been used most commonly in industry. In addition, phosphate nanopowders are a diverse class of compounds that can be used in a variety of applications [4]. The complex structure of phosphate compounds allows them to be distributed in several locations as divalent and trivalent cations [5]. Since phosphate compounds can be readily obtained, are environmentally friendly and simple to synthesize, and have a high band gap, low phonon frequency, good charge, and thermal stability, they can function as essential host materials in luminescent materials [6-9]. Luminescent materials commonly use rare earth metal ions (RE) as activators [10]. LEDs, displays, wave guiding lasers, scintillators, detectors, solid-state lasers, and fiber-optic amplifiers used for optical data storage, X-ray imaging, and underwater communications have been thoroughly tested with phosphate nanopowders. Ln^{3+} or Sm^{3+} ions are commonly utilized as activators in most nanopowders [11]. LEDs are poised to revolutionize lighting because of their adaptability, great efficiency, and ability to store energy. Chromaticity coordinates, color rendering

*Corresponding author. E-mail: sandhya.cole@gmail.com

index (CRI), color-correlated temperature (CCT), and color purity all influence the power of a phosphor to produce light [12]. In the present study, cadmium-strontium phosphate ($Cd_2Sr(PO_4)_2$; CSP in short) nanopowder was prepared through a solid state reaction (SSR), and its structural, optical (luminescence), and morphological properties were studied. Additionally, the Commission Internationale de l' Éclairage (CIE) 1931 colorimetric standard was used to calculate factors such as CRI, CCT, and color purity.

METHODS AND MATERIALS

Ammonium dihydrogen orthophosphate ($NH_4H_2PO_4$, 99.9%), cadmium oxide (CdO, 99.9%), strontium carbonate ($SrCO_3$, 99.99%), and samarium oxide (Sm_2O_3) were combined and used to synthesize the Sm_2O_3-doped CSP nanopowder by the SSR method. This method involved repeated intermediate grinding and sintering for two hours at 500 °C and 1000 °C in a programmed muffle furnace. The prepared sample was crushed to a fine powder for two hours to obtain an ultrafine nanopowder. The synthesis method is represented chronologically in Fig. 1.

CHARACTERIZATION

The powder X-ray diffraction studies (P-XRD) pattern for Sm^{3+}-doped CSP nanopowder was recorded using a Rigaku Miniflex 600 model X-ray instrument at the Cu-kα wavelength (λ = 0.15406 nm) and in the range of 2θ = 5° to 90° with a step size 0.02°. Scanning electron microscopy

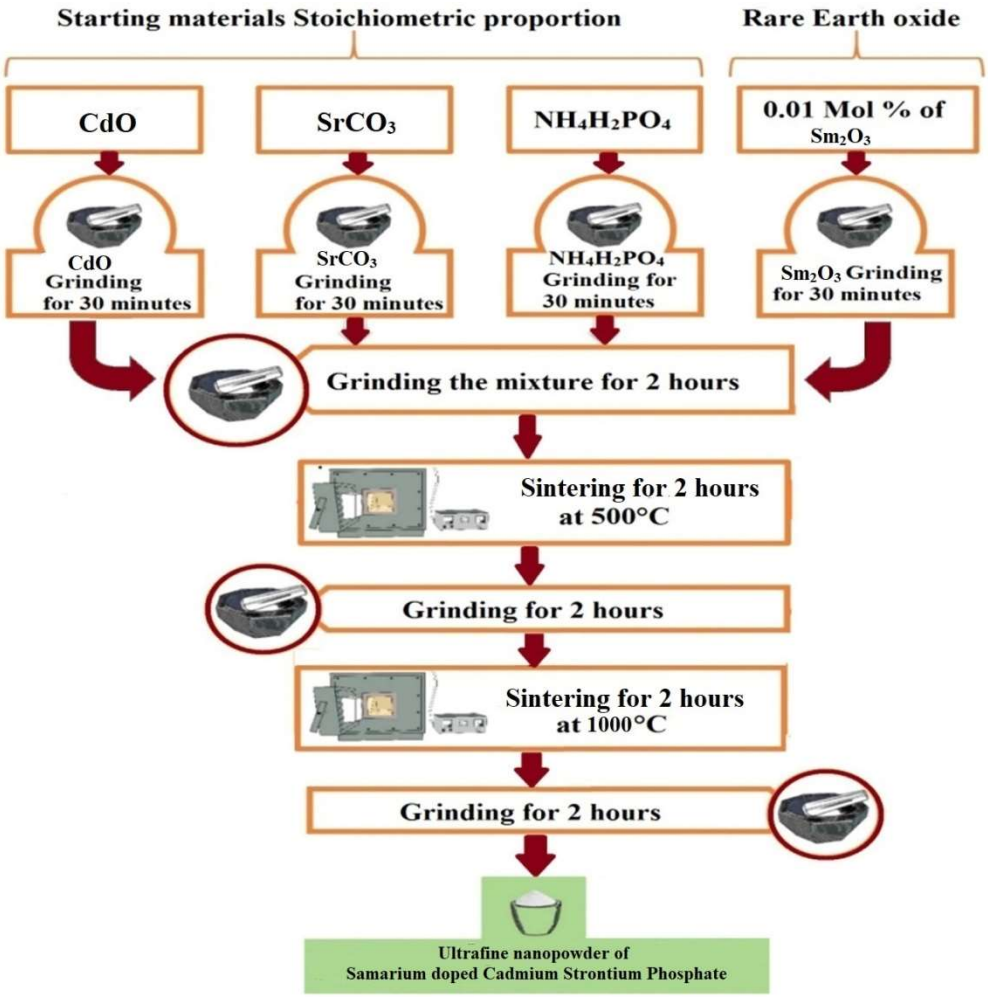

Fig. 1. The schematic representation of the synthesis of Sm^{3+}-doped CSP nanopowder by the SSR method.

(SEM) micrographs and energy dispersive X-ray spectroscopy (EDS) elemental mapping pictures were obtained using a JEOL JSM-IT-500 (Japan) instrument equipped with an EDS facility. The diffuse reflectance spectrum (DRS) of the prepared sample was recorded in the region of 200-1200 nm using a UV/Vis/NIR-DRS spectrophotometer (SPECORD-210 Plus-Analytik Jena, Japan). The Fourier transform infrared spectroscopy (FT-IR) spectrum of the prepared sample was collected from a Bruker ALPHA II FT-IR spectrometer in the range of 4000-400 cm^{-1} by the KBr pellet method. The luminescence spectrum of the prepared sample was recorded using a Perkin Elmer LS 55 spectrometer fitted with a xenon lamp.

RESULTS AND DISCUSSION

P X-Ray Diffraction Studies

Figure 2 represents a sharp peaks in the P-XRD pattern of Sm^{3+}-doped CSP nanopowder. Moreover, well-defined, clear, prominent peaks can be seen in Fig. 2; these peaks were well indexed to JCPDS card No. 00-054-0979. Debye–Scherrer's Eq. (1) [13-14] was used to estimate the average crystallite size of the synthesized sample. The following equations [15-17] were used to calculate the microstrain (Eq. (2)) and dislocation density (Eq. (3)).

$$D = \frac{K\lambda}{\beta cos\theta} \quad (1)$$

$$\varepsilon = \frac{\beta}{4\, tan\theta} \quad (2)$$

$$\delta = \frac{1}{D^2} \quad (3)$$

where D is the average size of the crystallite, δ is the density of dislocation, ε is the microstrain, K is the shape factor, λ is X-rays wave length, θ is Bragg's diffraction angle, and β is full width half maxima.

The crystallite size (D), microstrain (ε), and dislocation density (δ) were calculated using the above equations and their values were 15 nm, 68 × 10^{-4}, and 4.4 × 10^{15} lines/m^2, respectively.

Williamson-Hall (W-H) Method

The W-H plot was employed to estimate the microstrain

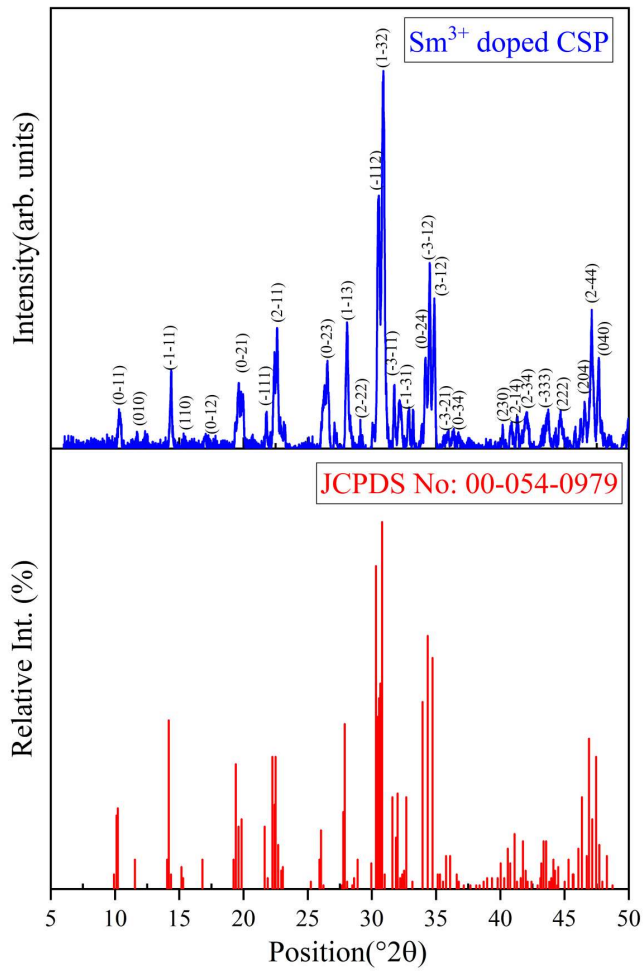

Fig. 2. The P-XRD pattern of Sm^{3+}-doped CSP.

(ε) and the crystallite size (D). In addition, the dislocation density (δ) was calculated based on the crystallite size. These three parameters were calculated using the following equation (Eq. (4)).

$$\beta cos\theta = (0.9\lambda/D) + 4\varepsilon sin\theta \quad (4)$$

In the W-H method, as shown in Fig. 3, a plot was drawn between 4 sinθ (on X-axis) and βcosθ (on Y-axis). The plot was a straight line that did not pass through the origin (y = mx + c). From the line equation, the division of kλ by the intercept gave the crystallite size, and the slope of the straight line represented the microstrain. Based on the W-H plot, the following results were drawn: D = 16 nm, ε = 94 ×

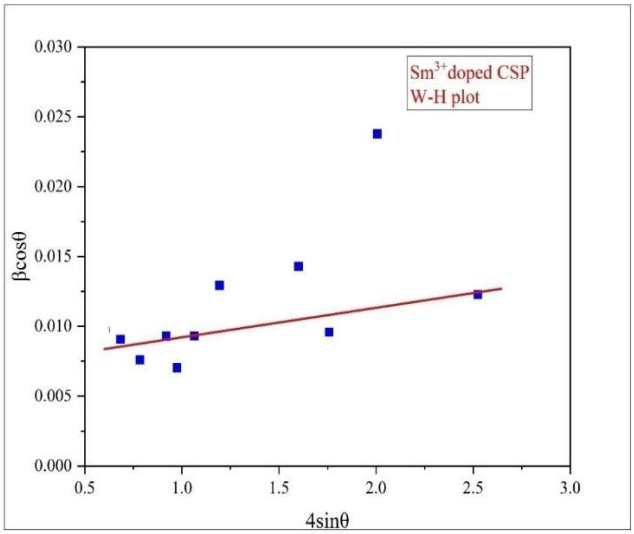

Fig. 3. The W-H plot of Sm^{3+}-doped CSP.

Table 1. A Comparison of D, ε, and δ Values Calculated from the P-XRD Pattern of Sm^{3+}-doped CSP Nanopowder

No.	Parameter	Debye-Scherer's method	W-H method
1	Size of crystallite (D)	15 nm	16 nm
2	Micro strain (ε)	68×10^{-4}	94×10^{-4}
3	Dislocation density (δ)	4.4×10^{15} lines/m^2	3.9×10^{15} lines/m^2

10^{-4}, and $\delta = 3.9 \times 10^{15}$ lines/m^2. A comparison of the values of these three parameters calculated by the Debye-Scherrer's equation and the W-H plot is shown in Table 1.

SEM with EDS

In Figs. 4(a-d), the SEM images of CSP nanopowder doped with Sm^{3+} ions are shown. Figure 4(a-d) shows the formation of agglomerates with biscuit-like non-uniform nanoflakes. These micrographs revealed flakes that resembled biscuits. The measurements were carried out in various resolutions. Figure 4e depicts the EDS spectrum used to determine the composition information of the prepared sample and its different elemental compositions.

Cadmium, strontium, phosphorous, oxygen, and samarium exhibited separate peaks in the EDS spectrum. The samarium content in the CSP nanopowder was 15.62 wt.% and 4.39 atomic% [18], confirming the presence of dopant ions in the synthesized sample [19].

The DRS Study

The DRS of Sm^{3+}-doped $Cd_2Sr(PO_4)_2$ was collected in the wavelength range of 200-1200 nm. Based on this reflection data, the Kubelka-Munk function was employed to derive the absorption (K/S) values. The Kubelka-Munk function [20-21] is presented below:

$$F(R) = K/S = (1 - R)^2/2R,$$

where K is the absorption coefficient, S is the scattering coefficient, and R is the reflectivity of the sample. A graph plotted between $[F(R)h\upsilon]^2$ *vs.* $h\upsilon$ is shown in Fig. 5. The band gap value was estimated as $E_g = 5.3$ eV, confirming the band gap value reported in previous studies [22]. The wide band gap value of the prepared sample suggests that the prepared sample can be used in device applications, such as LEDs [20] and solar cells.

FT-IR Study

In the wavelength range of 4000-400 cm^{-1}, FT-IR was recorded to determine the primary bands of vibration present in the Sm^{3+}-doped CSP nanopowder. Figure 6, which shows the FT-IR spectra of CSP, represents different asymmetric and symmetric vibrational modes of bending and stretching related to the prepared sample. Two bands observed at 956 and 976 cm^{-1} were associated with the symmetric stretching mode of PO_4^{3-} ions (ν_1) [20]. The group of bands observed at 1002, 1040, 1070, and 1106 cm^{-1} corresponded to the asymmetric stretching mode of PO_4^{3-} ions (ν_3) [24]. The three bands observed at 430, 482, and 497 cm^{-1} corresponded to the asymmetric bending mode of PO_4^{3-} ions (ν_2) [20]. The two bands observed at 557 and 576 cm^{-1} corresponded to the symmetric bending mode of PO_4^{3-} ions (ν_4) [25]. An infrared band observed at 740 cm^{-1} corresponded to the symmetric stretching mode of the P-O-P bridge [26]. The FT-IR spectrum analysis confirmed the presence of ions related to phosphate groups in the sample.

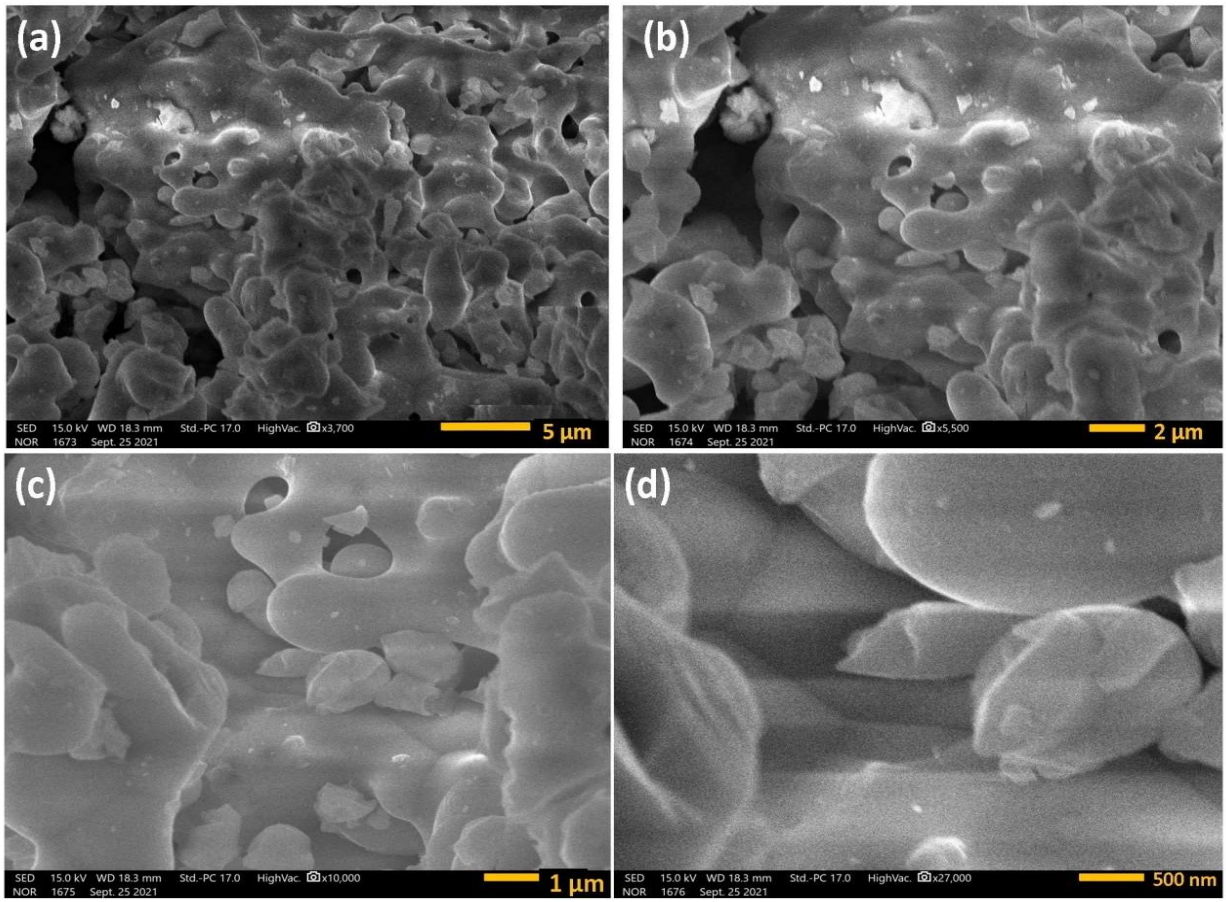

Fig. 4a-d. The SEM images of CSP nanopowder doped with Sm^{3+} ion.

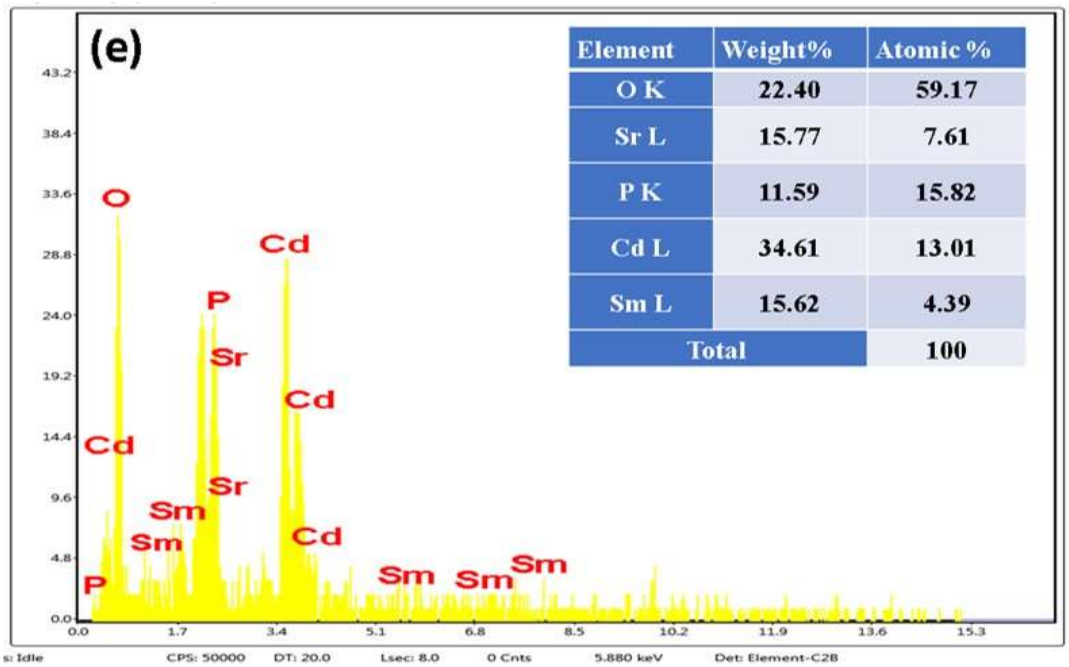

Element	Weight%	Atomic %
O K	22.40	59.17
Sr L	15.77	7.61
P K	11.59	15.82
Cd L	34.61	13.01
Sm L	15.62	4.39
Total		100

Fig. 4e. The EDS spectrum of CSP nanopowder doped with Sm^{3+} ion.

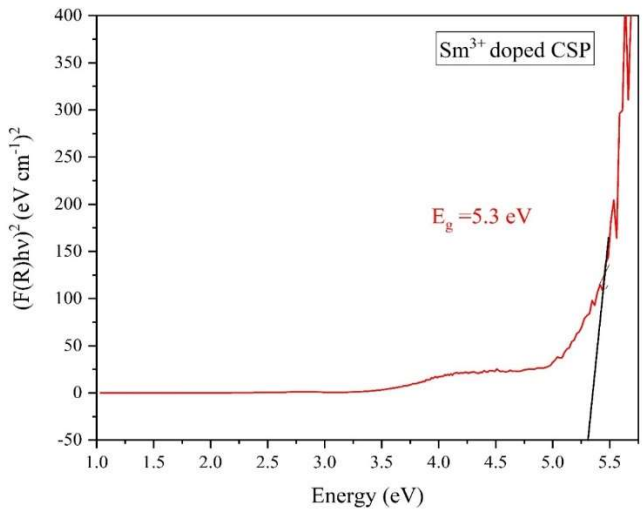

Fig. 5. The Kubelka-Munk plot of Sm^{3+}-doped CSP nanopowder.

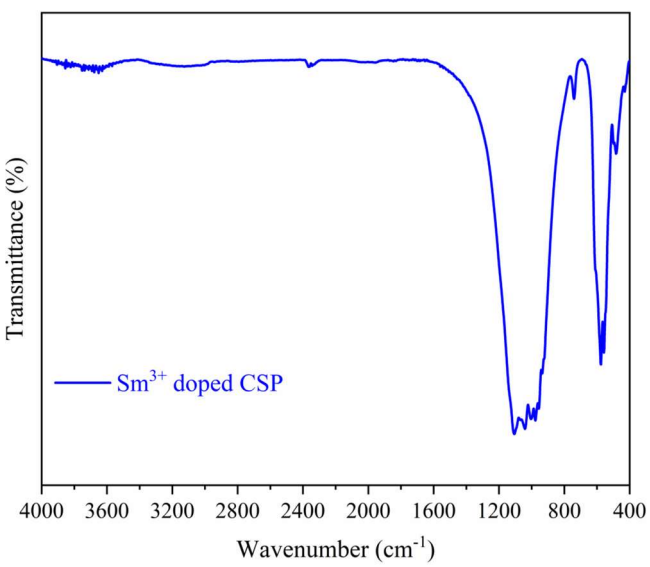

Fig. 6. The FT-IR spectrum of Sm^{3+}-doped CSP nanopowder.

Table 2. CIE Color Coordinates, CCT, CRI, and Color Purity of Sm^{3+}-Doped CSP Nanopowder

Compound	CC (x_s, y_s)	CCT (K)	CRI (%)	CP (%)
Sm^{3+}-doped CSP	(0.5097, 0.4748)	2546	58	95.6

Photoluminescence (PL)

The PL emission spectrum of CSP nanopowder doped with Sm^{3+} ion was monitored at 596 nm and a peak was observed upon excitation at 401 nm (Fig. 7). The emission spectrum of CSP nanopowder doped with Sm^{3+} is given in Fig. 8a. Four sharp peaks assigned to 564 nm ($^4G_{5/2}\rightarrow{}^6H_{5/2}$), 596 nm ($^4G_{5/2}\rightarrow{}^6H_{7/2}$), 643 nm ($^4G_{5/2}\rightarrow{}^6H_{9/2}$), and 704 nm ($^4G_{5/2}\rightarrow{}^6H_{11/2}$) transitions were seen in the emission spectra [27]. Color displays, high-density optical storage, and medical diagnostics are just a few of the applications that stand to gain from these transitions between energy levels shown in the PL spectrum. The energy level diagram of Sm^{3+}-doped CSP nanopowder is shown in Fig. 8b. The maximum intensity peak at 596 nm ($^4G_{5/2}\rightarrow{}^6H_{7/2}$) was situated in the orange region [28-29]. The luminescence intensity ratio between electric dipole (ED) and magnetic dipole (MD) transitions can be used to determine the local environment of trivalent $4f^s$ ions. The ($^4G_{5/2}\rightarrow{}^6H_{5/2}$) was an allowed MD transition and ($^4G_{5/2}\rightarrow{}^6H_{9/2}$) was an allowed ED transition [30] whereas ($^4G_{5/2}\rightarrow{}^6H_{7/2}$) was an allowed MD and ED transition owing to the selection condition $J = \pm 1$. This latter transition was extremely sensitive to the Sm^{3+} ions due to its hypersensitivity. There is an increased asymmetry in ED transition with higher intensity. According to the present study, there was a greater asymmetry in the spectral intensity of Sm^{3+} ions of the ($^4G_{5/2}\rightarrow{}^6H_{9/2}$) ED transition than ($^4G_{5/2}\rightarrow{}^6H_{5/2}$) MD transition [31].

Photometric Analysis

Figure 9 shows the CIE chromaticity diagram of CSP nanopowder doped with Sm^{3+}. The CIE chromaticity coordinates were calculated using the emission spectral values of Sm^{3+}-doped CSP powder and the color calculator program (version 7.77), and the coordinates were 0.5097, 0.4748 [31]. The coordinates were located in the orange region. An empirical formula developed by McCamy (Eq. (5)) was used to determine the CCT [32-33].

$$CCT = -437n^3 + 3607n^2 - 6861n + 5514.31 \quad (5)$$

where n = color chromaticity = $(x - x_e)/(y - y_e)$ and epicenter (x_e, y_e) = (0.5097, 0.4748).

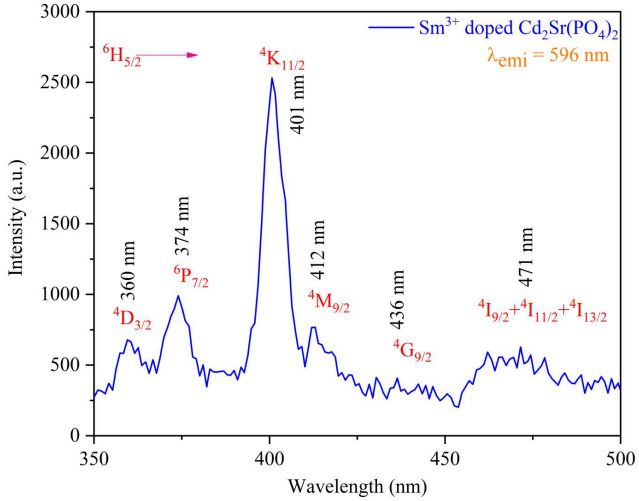

Fig. 7. The PL spectrum of Sm^{3+}-doped CSP nanopowder upon excitation.

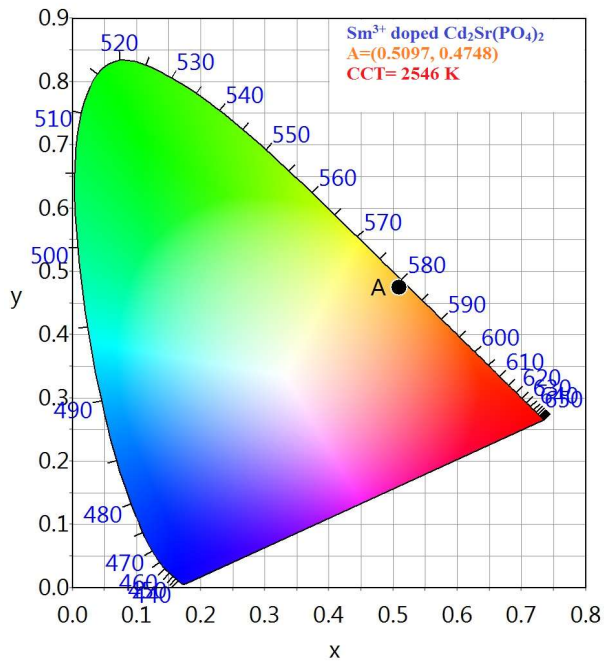

Fig. 9. The CIE diagram of Sm^{3+}-doped CSP nanopowder.

Color purity was determined by the following formula:

$$\text{Color purity} = \frac{\sqrt{(x_s - x_i)+(y_s - y_i)}}{\sqrt{(x_d - x_i)+(y_d - y_i)}}$$

There was a correspondence between the coordinates of the sample point and the coordinates of the point of illumination as well as the dominant wavelength.

CRI is one of the most important photometric tools for analyzing emission spectrum data and a quantitative measure of the ability of a light source to reproduce the colors of various objects faithfully compared with a natural or standard light source. Light sources with a high CRI are desirable in color-critical applications, such as neonatal care and art restoration. Sm^{3+}-doped CSP nanopowder has a decent light output CRI (*i.e.,* 58%), which is equivalent to saturation when considering the XY chromaticity, which describes how pure or monochromatic a light source is. The sample color

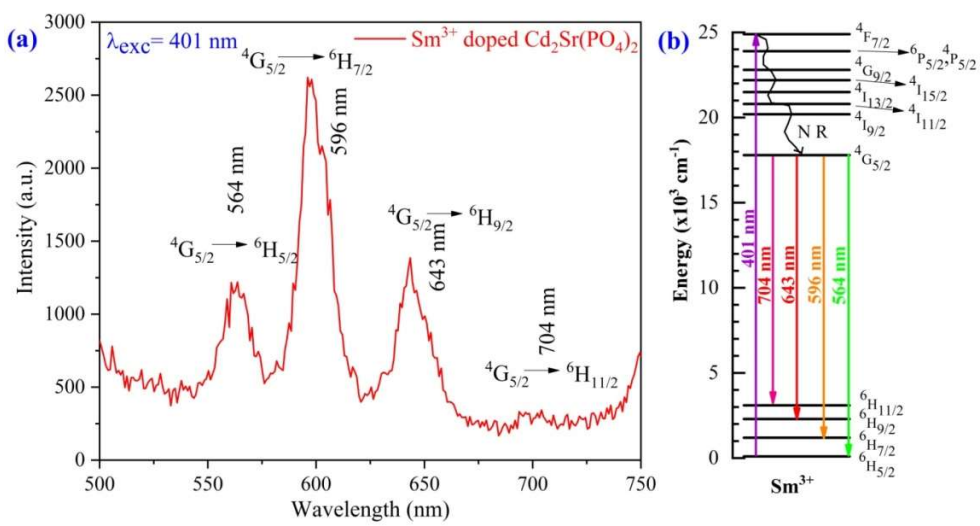

Fig. 8. (a) The PL emission spectrum (b) energy level diagram of Sm^{3+}-doped CSP nanopowder.

purity was 95.6%. Synthesized materials can be used as LEDs and optical sensors (photo-responsive devices) that produce warm light. Relative statistics for each estimated photometric parameter of the prepared sample are shown in Table 2.

CONCLUSIONS

The SSR method was used to synthesize the Sm^{3+}-doped CSP. The P-XRD analysis showed that the sample had a crystallite size of 15 nm. The SEM and EDS analyses revealed that the sample had non-uniformly dispersed nanoflakes that resembled biscuits. Based on the DRS, the band gap was 5.3 eV. Phosphate ions and other precursor vibrational modes were discovered in FT-IR spectroscopy. According to the PL results, ($^4G_{5/2}\rightarrow{}^6H_{7/2}$) transition released an intense orange luminescence with an emission peak at 596 nm. The CIE chromaticity coordinates (0.5097, 0.4748) were found to be in the orange region for the prepared sample. The CCT, CRI, and color purity calculated values for the prepared sample were 2546 K, 58%, and 95.6%, respectively. Thus, it can be concluded that the prepared sample can have potential applications in LEDs and other warm-light emitting devices.

REFERENCES

[1] Bati, A. S. R.; Yu, L.; Batmunkh, M.; Shapter, J. G., Recent Advances in Applications of Sorted Single-Walled Carbon Nanotubes. *Adv. Funct. Mater.* **2019**, *29*, 1902273, https://doi.org/10.1002/adfm.201902273.

[2] Khidhirbrahmendra, V.; Basha, S.; Avinash, M.; Thampy, U.; Reddy, C.; Ravikumar, R., Investigations on structural and spectral properties of undoped and Mn^{2+} doped $SrZn_2(PO_4)_2$ nanophosphors for light emitting devices. *J. Mater. Sci. Mater. Electron.* **2019**, *30*, 5120-5129, https://doi.org/10.1007/s10854-019-00810-6.

[3] Huang, C.; Chen, X.; Xue, Z.; Wang, T. Effect of structure: A new insight into nanoparticle assemblies from inanimate to animate. *Sci. Adv.* **2020**, *6*, eaba1321, https://doi.org/10.1126/sciadv.aba1321.

[4] Muswareen, S. K. K.; Rao, M. S.; Sridevi, G.; Cole, S., Sol-gel synthesis of pure and TiO_2 doped $CdOFePO_4$ nanocomposites and investigation of their structural and optical properties. *Mater. Sci. Semicond. Process.* **2019**, *102*, 104588, https://doi.org/10.1016/j.mssp.2019.104588.

[5] Rao, M. S.; Satyavathi, K.; Bhaskararao, Y. N.; Cole, S., Structural and spectral investigations of undoped and Mn^{2+} ion doped Zn_3 $(PO_4)_2ZnO$ nanocrystalline phosphor materials. *J. Alloys Compd.* **2016**, *682*, 7-13, https://doi.org/10.1016/j.jallcom.2016.04.201.

[6] Gupta, S. K.; Ghosh, P. S.; Yadav, A. K.; Jha, S. N.; Bhattacharyya, D.; Kadam, R. M., Origin of blue-green emission in α-$Zn_2P_2O_7$ and local structure of Ln^{3+} ion in α-$Zn_2P_2O_7$: Ln^{3+} (Ln = Sm, Eu): time-resolved photoluminescence, EXAFS, and DFT measurements. *Inorg. Chem.* **2017**, *56*, 167-178, https://doi.org/10.1021/acs.inorgchem.6b01788.

[7] Mahajan, R.; Prakash, R. Effect of Sm^{3+} doping on optical properties of $Mg_2P_2O_7$ and $Mg_3P_2O_8$ phosphors. *Mater. Chem. Phys.* **2020**, *246*, 122826, https://doi.org/10.1016/j.matchemphys.2020.122826.

[8] Wang, Z.; Xia, Z.; Molokeev, M. S.; Atuchin, V. V.; Liu, Q., Blue-shift of Eu^{2+} emission in $(Ba, Sr)_3$ Lu $(PO_4)_3$: Eu^{2+} eulytite solid-solution phosphors resulting from release of neighbouring-cation-induced stress. *Dalton Trans.* **2014**, *43*, 16800-16804, https://doi.org/10.1039/C4DT02319F

[9] Rajyalakshmi, T.; Basha, S. J.; Khidhirbrahmendra, V.; Krishna, A. G.; Ravikumar, R., Synthesis and spectroscopic investigations of calcium cadmium phosphate hydrate nanopowders *via* doping divalent (Mn^{2+}) and trivalent (Fe^{3+}) cations. *J. Mol. Struct.* **2020**, *1222*, 128929, https://doi.org/10.1016/j.molstruc.2020.128929.

[10] Zhong, Y.; Deng, B.; Gao, X.; Sun, P.; Ren, Y.; Liang, T.; Yu, R., High thermally Sm^{3+}-activated $SrBi_2Ta_2O_9$ orange-red phosphor: Preparation, characterization, and optical properties. *J. Lumin.* **2019**, *215*, 116648, https://doi.org/10.1016/j.jlumin.2019.116648.

[11] Ji, H.; Huang, Z.; Xia, Z.; Molokeev, M. S.; Chen, M.; Atuchin, V. V.; Fang, M.; Liu, Y. G.; Wu, X., Phase Transformation in $Ca_3(PO_4)_2$:Eu^{2+} *via* the Controlled Quenching and Increased Eu^{2+} Content: Identification of New Cyan-Emitting α-$Ca_3(PO_4)_2$:Eu^{2+} Phosphor. *J. Am. Ceram. Soc* . **2015**, *98*, 3280-3284,

https://doi.org/10.1111/jace.13787,

[12] Krishnan, R.; Swart, H.; Thirumalai, J.; Peter, A. J., Synthesis of self-assembled micro flowers of ($Na_{0.5}La_{0.5}$) MoO_4: Eu^{3+} phosphor and it's photometric properties. *Mater. Lett.* **2019**, *243*, 58-61, https://doi.org/10.1016/j.matlet.2019.01.156.

[13] Venkatarao, K.; Sreedevi, G.; Rajeev, Y. N.; Cole, S. Impact of TiO_2 on structural and spectral properties of ZnS-MoS_2 nanocomposites. *Mater. Today: Proc.* **2022**, *49*, A12-A18, https://doi.org/10.1016/j.matpr.2021.12.386.

[14] Kumar, B. V. N.; Balla, P. K.; Chirauri, S. K.; Rao, T. K. V.; Ramakrishna, Y.; Rao, K. R., Synthesis and characterization of copper particles decorated reduced graphene oxide nano composites for the application of supercapacitors. *AIP Conf. Proc.* **2018**, *1992*, 040008, https://doi.org/10.1063/1.5047973.

[15] Sreedevi, G.; Muswareen, S. K. K.; Jayalakshmi, V.; Cole, S., Effect of TiO_2 doping on structural and optical properties of $CdSZn_3(PO_4)_2$ nanocomposites. *Appl. Phys. A* **2019**, *125*, 741, https://doi.org/10.1007/s00339-019-3037-3.

[16] Satyavathi, K.; Rao, M. S.; Nagabhaskararao, Y.; Cole, S., Synthesis, characterization of undoped and doped Zn_3 $(PO_4)_2ZnO$ nanopowders by sol–gel method. *J. Mater. Sci. Mater.* **2017**, *28*, 12226-12238, https://doi.org/10.1007/s10854-017-7038-8

[17] Bhaskararao, Y. N.; Satyavathi, K.; Rao, M. S.; Cole, S., Synthesis and characterization of Mn^{2+} doped $CdOZn_3(PO_4)_2$ nanocomposites. *J. Mol. Struct.* **2017**, *1130*, 585-591, https://doi.org/10.1016/j.molstruc.2016.11.031.

[18] Balla, P. K.; Kumar, B. V. N.; Ganesan, K.; Shaik, E. B.; Rao, K. R., Nano casting fabrication of porous N-doped carbon using melamine-formaldehyde resins. *AIP Conf. Proc.* **2018**, *1992*, 040016, https://doi.org/10.1063/1.5047981.

[19] Arasi, S. E.; Madhavan, J.; Antony Raj, M. V., Effect of samarium (Sm^{3+}) doping on structural, optical properties and photocatalytic activity of titanium dioxide nanoparticles. *J. Taibah Univ. Sci.* **2018**, *12*, 186-190, https://doi.org/10.1080/16583655.2018.1451057.

[20] Sarathkumar, S.; Munimasthani, S.; Thampy, U. S. U.; Ravikumar, R. V. S. S. N.. Structural and luminescent properties of $CaZn_2(PO_4)_2$: RE^{3+} (RE = Er and Pr) nanophosphors for versatile device applications. *J. Mater. Sci. Mater. Electron.* **2020**, *31*, 11589-11598, https://doi.org/10.1007/s10854-020-03707-x.

[21] Munimasthani, S.; Sarathkumar, S.; Udaychandran Thampy, U. S.; Ravikumar, R., Structural and luminescence studies of Dy^{3+}-activated cadmium calcium pyrophosphate. *Appl. Phys. A* **2020**, *126*, 1-7, https://doi.org/10.1007/s00339-019-3180-x.

[22] Munimasthani, S.; Sarathkumar, S.; Reddy, N. B.; Zyryanov, G. V.; Ravikumar, R., Luminescence studies on Pr^{3+} and Yb^{3+} doped cadmium calcium pyrophosphate nanophosphors. *AIP Conf. Proc.* **2020**, *2280*, 040034, https://doi.org/10.1063/5.0018043.

[23] Rajyalakshmi, T.; Basha, S. J.; Khidhirbrahmendra, V.; Thampy, U. S. U.; Ravikumar, R. V. S. S. N., Synthesis and investigations for white LED material: VO^{2+} doped Calcium Cadmium phosphate hydrate nanophosphor. *J. Mol. Struct.* **2020**, *1205*, 127605, https://doi.org/10.1016/j.molstruc.2019.127605.

[24] Frost, R. L.; Scholz, R.; López, A.; Xi, Y., A vibrational spectroscopic study of the phosphate mineral whiteite $CaMn^{++}Mg_2Al_2(PO_4)_4(OH)_2{\cdot}8(H_2O)$. *Spectrochim. Acta A Mol. Biomol. Spectrosc.* **2014**, *124*, 243-248, https://doi.org/10.1016/j.saa.2014.01.053.

[25] Sarathkumar, S.; Munimasthani, S.; Thampy, U. S.; Ravikumar, R., Structural and luminescent properties of $CaZn_2(PO_4)_2$: RE^{3+} (RE = Er and Pr) nanophosphors for versatile device applications. *J. Mater. Sci.: Mater. Electron.* **2020**, *31*, 11589-11598, https://doi.org/10.1007/s10854-020-03707-x.

[26] Munimasthani, S.; Sarathkumar, S.; Khidhirbrahmendra, V.; Ravikumar, R. V. S. S. N., Structural studies of Nd^{3+} doped cadmium calcium pyrophosphate nanophosphors. *Mater. Today: Proc.* **2020**, *26*, 114-116, https://doi.org/10.1016/j.matpr.2019.05.445.

[27] Wei, Q.; Zheng, Z. -P.; Feng, H. -X.; Hong, X. -J.; Huang, X.; Peng, H. -J.; Cai, Y. -P., Two samarium(III) complexes with tunable fluorescence from *in situ* reactions of 2-ethoxy-6-((pyridin-2-ylmethylimino)methyl)phenol with Sm^{3+} ion. *RSC Adv.* **2016**, *6*, 94687-94691,

https://doi.org/10.1039/C6RA20957B.

[28] Munimasthani, S.; Sarathkumar, S.; Reddy, N. B.; Zyryanov, G. V.; Ravikumar, R. V. S. S. N., Luminescence studies on Pr^{3+} and Yb^{3+} doped cadmium calcium pyrophosphate nanophosphors. *AIP Conf. Proc.* **2020**, *2280*, 040034, https://doi.org/10.1063/5.0018043.

[29] Reddy, C. P.; Naresh, V.; Babu, B. C.; Buddhudu, S., Photoluminescence and energy transfer process in Bi^{3+}/Sm^{3+} co-doped phosphate zinc lithium glasses. *Adv. Mater. Phys. Chem.* **2014**, *4*, 165, https://doi.org/10.4236/ampc.2014.49019.

[30] Xin, M.; Tu, D.; Zhu, H.; Luo, W.; Liu, Z.; Huang, P.; Li, R.; Cao, Y.; Chen, X., Single-composition white-emitting $NaSrBO_3$: Ce^{3+}, Sm^{3+}, Tb^{3+} phosphors for NUV light-emitting diodes. *J. Mater. Chem. C* **2015**, *3*, 7286-7293, https://doi.org/10.1111/j.1551-2916.2005.00532.x.

[31] Rajeev, Y. N.; Venkatarao, K.; Kumar, B. V. N.; Kumar, L. B.; Cole, S., Structural, morphological and luminescent studies on Sm^{3+} doped strontium tin phosphate nanopowder. *Mater. Today: Proc.* **2022**, *49*, A1-A6, https://doi.org/10.1016/j.matpr.2021.12.554.

[32] Sreedevi, G.; Srinivas, K.; Subbarao, M.; Cole, S., Investigation on structural and optical properties of CuO doped CdS-$Zn_3(PO_4)_2$ nanocomposite for optoelectronic devices. *J. Mol. Struct.* **2020**, *1222*, 128903, https://doi.org/10.1016/j.molstruc.2020.128903.

[33] Nirmal Rajeev, Y.; Venkatarao, K.; Naveen Kumar, B. V.; Bhushan Kumar, L.; Cole, S., Structural and Morphological Studies on Strontium Tin Phosphate $SrSn(PO_4)_2$ Nanopowder. *Phys. Chem. Res.* **2022**, *10*, 267-271, https://doi.org/10.22036/pcr.2021.300514.1953.